International Journal of
INTELLIGENT SYSTEMS AND APPLICATIONS IN ENGINEERING
ISSN:2147-6799 www.ijisae.org Original Research Paper

Mechanical and Microstructural Evaluation of Fly Ash–GGBFS Alkali Activators Reinforced with Steel and Polypropylene Fibers

Amit Kumar[1], **Dr. N.P Kaushik**[2]

Submitted:18/08/2025 **Revised:**30/09/2025 **Accepted:**10/10/2025

Abstract: The experimental investigation was carried out to examine how polypropylene (PP) and steel Fibers (SF) influence the microstructural characteristics and mechanical response of fly ash (FA) and ground granulated blast furnace slag (GGBFS)–based alkali-activated mortars. In this study, FA and GGBFS, both obtained as industrial by-products, served as the main aluminosilicate precursors for synthesizing the binder matrix. Various Fiber volume fractions of PP and SF were incorporated to evaluate their effects on compressive strength, splitting tensile strength, and flexural performance. The compressive elastic modulus was estimated using an empirical model derived from the experimentally determined compressive strength (CS) values of the Fiber-reinforced mixtures. Results revealed that adding PP Fibers up to approximately 2.35% by volume led to a notable enhancement in flexural strength and deformation resistance. On the other hand, incorporating 2.25% SF resulted in the highest compressive strength, showing an improvement of 14.15% compared with the control mix. Both PP- and SF-reinforced mortars displayed a progressive rise in flexural toughness index with increasing Fiber dosage, although the enhancement was more pronounced in the SF composites, highlighting their superior crack-bridging efficiency and energy absorption capacity.

Keywords: *Fiber-reinforced alkali activators, Fly Ash, GGBFS, Mechanical properties, Flexural toughness, Elastic modulus, Microstructure*

1. Introduction

The construction industry is continuously evolving to meet modern infrastructural demands that align with global standards for sustainable development. To satisfy these growing needs, cement production has risen sharply, particularly in developing nations such as India, which together account for more than half of the world's cement output in 2024–2025 [1]. Despite its widespread use, cement manufacturing poses significant environmental challenges due to its considerable carbon dioxide (CO_2) emissions. It is estimated that the cement industry alone contributes nearly 5% of total global CO_2 emissions [2], making it one of the leading sources of anthropogenic greenhouse gases. Alongside this issue, the accumulation and improper disposal of industrial by-products, such as FA, have emerged as additional environmental concerns. To mitigate these challenges, researchers have been actively exploring alternative binders that can replace conventional cement while reducing ecological impact [3]. Among the various substitutes investigated, alkali activators have gained notable attention for their environmental and technical advantages. These materials utilize industrial residues as primary aluminosilicate sources, significantly minimizing the carbon footprint associated with traditional cement production [4]. Alkali activator technology has therefore emerged as a sustainable solution for waste utilization and CO_2 emission reduction. In recent years, there has been a rapid advancement in the development of alkali activator-based construction materials as viable alternatives to ordinary Portland cement (OPC) [5]. Globally, alkali activators are recognized for their superior mechanical strength and durability characteristics, which make them promising candidates for structural and infrastructural applications [6]. When activated by alkaline solutions, these materials undergo polymerization reactions involving the formation of Si–O–Al–O chains, resulting in a dense and stable aluminosilicate network [7].

FA, an abundant derivative generated globally from coal combustion, possesses high pozzolanic reactivity and has been extensively utilized in construction applications. Due to its chemical composition and fine particle size, FA-based binders exhibit superior performance compared with conventional ordinary Portland cement (OPC) systems. Consequently, numerous studies have examined the mechanical, durability, and microstructural characteristics of FA-based alkali activator materials [8]. In addition, several investigations have highlighted the beneficial influence of ground granulated blast furnace slag (GGBFS) on the strength development of FA–based alkali activators, particularly under ambient curing conditions [9]. Despite these advantages, prior research consistently indicates that alkali activator composites, similar to OPC concrete, exhibit a quasi-brittle failure pattern, limiting their tensile load-carrying capacity. To address this drawback, recent research has focused on developing fiber-reinforced alkali activator systems to boost toughness and crack resistance for broader structural demand. Amalgamation of fibers—such as steel, polypropylene (PP), silica, and other inorganic fibers—has been shown to improve the tensile and flexural behavior of alkali activator composites [10]. Mechanical strength significantly improved the durability performance of alkali activators compared with traditional cement-based materials. Their findings demonstrated that both plain and fiber-reinforced alkali activator specimens exhibited superior deformation capacity and post-cracking behavior relative to OPC composites. However, the incorporation of higher fiber volumes in concrete mixtures can adversely affect workability and, in some

1 OM Sterling Global University, Haryana, India
ORCID ID : 0009-0007-1334-6560
** Corresponding Author Email: amitbamal07@gmail.com*

cases, CS, thereby necessitating optimization of fiber dosage for practical applications [11].

In another study, Bernal et al. (2010) [12] examined slag-based alkali activators reinforced with SF to assess their mechanical and durability characteristics. Their results demonstrated that steel fiber inclusion substantially increased flexural strength and overall durability, although a marginal depletion in CS was discover at higher fiber contents. Mechanical behavior and impact of lightweight alkali activator composites reinforced with SF and revealed improvements in flexural and splitting tensile strengths by approximately 38% and 30%, compared to the control mix. Moreover, SF incorporation significantly boostd the impact load resistance of the alkali activator composites [13]. A combination of SF and PP fibers shows effect on FA-based alkali activator mortars, noting that SF produced superior flexural strength compared with PP fibers. The study also highlighted that oven-cured specimens exhibited better performance than those cured under ambient conditions. Although PP fibers did not markedly influence CS, they contributed positively to tensile and flexural properties [14]. Previous investigations have consistently shown that PP fiber inclusion improves splitting tensile and flexural strengths, reduces shrinkage, and boosts the creep behavior of alkali activator composites.

Although the inclusion of SF is known to boost the mechanical properties, particularly CS and flexural stiffness—of alkali activator composites, other types of fibers have also been explored for performance improvement. Several studies have focused on polyvinyl alcohol (PVA) fiber-reinforced alkali activators to assess their mechanical and durability characteristics. For instance, Xu et al. (2017) [15] investigated the flexural behavior of FA-based alkali activator composites reinforced with PVA fibers and reported substantial improvements in mechanical properties compared with the control mix. Their findings also revealed that longer PVA fibers provided superior toughness and strength due to improved stress transfer mechanisms within the matrix.

The overall performance of fiber-reinforced alkali activator composites is influenced by multiple parameters, including fiber type, content, binder composition, curing conditions, and curing age [16]. Equally critical is the interfacial adhesion the fibers and the alkali activator binder, which governs load transfer efficiency and composite integrity. A well-developed interfacial transition zone (ITZ) between the reinforcement and the alkali activatoric matrix contributes to boostd load-bearing capacity [17]. In alkali-activated binders, the degree of wettability between the fibers and the alkaline activator significantly affects interfacial adhesion, leading to the formation of a stronger ITZ and improved mechanical response [18].

The present study examines the influence of PP and SF on performance of mechanical and microstructural characteristics with FA–GGBFS alkali activator. Alkali activator mortars were prepared by incorporating varying fiber volume dosage—0.75%, 1.0%, 1.75%, 2.0%, and 2.5%—for both PP and SF individually. A comparative investigation was carried out to assess the relative performance of the two fiber types. The elastic modulus was determined empirically based on experimental CS results, while the flexural toughness was assessed under applied load conditions.

Table 1 Chemical composition of FA and GGBFS.

Material	Al_2O_3	Fe_2O_3	SiO_2	CaO	MgO	Na_2O	K_2O	MnO	P_2O_5	SO_3	TiO_2	L LOI
FA	25.28	5.56	54.13	3.17	2.51	0.21	0.81	1.754	0.75	1.45	0.758	1.759
GGBFS	12.54	2.10	31.85	43.17	5.13	0.17	–	2.56	–	0.73	–	1.98

Table 2 PP and Steel fiber properties

Fiber type	Length: mm	Diameter: mm	Specific gravity	Tensile strength: MPa	Aspect ratio
PP	9	0.0075	0.9	774	1598
Steel	6	0.15	7.7	2051	35

2. Experimental program

2.1. Materials

In this research, industrial by-products—Class F FA and GGBFS—were utilized as primary binders in accordance with ASTM C618-19 [19] and ASTM C989-2018 [20]. The FA was procured from the National Thermal Power Corporation (NTPC), Vijayawada, whereas the GGBFS was sourced from Jaipur, Rajasthan, India. Table 1 contains the chemical makeup of FA and GGBFS. The specific gravity of FA was 2.27, and for GGBFS, it was 2.91. Their fineness values were 461 m^2/kg and 684 m^2/kg, respectively.

PP and SF were obtained from TATA Steel, Gujarat, India. Table 2 provides a summary of the comprehensive physical and geometrical characteristics of these fibers. To enhance the mechanical properties of alkali activator composites, short-length PP and SF were utilized. The selection of short fibers was based on their proven efficiency in improving strength and toughness, even at relatively low volume fractions. While small quantities of short fibers effectively boost strength characteristics, high fiber content causes poor dispersion and weak interfacial adhesion, resulting in reduced stiffness and strength.

The alkaline activator solution was prepared using sodium-based chemicals—sodium silicate (Na_2SiO_3) and sodium hydroxide (NaOH)—Purchased from Bangalore, India. The sodium silicate solution contained 29.2% SiO_2, 9.1% Na_2O, and 71.75% water, while NaOH pellets of >97.9% purity were used to prepare an 8 M solution. For all alkali activator mixes, the Na_2SiO_3 to NaOH ratio was maintained at 2.4:1, and the alkaline solution-to-binder (S/B) ratio was fixed at 0.35.

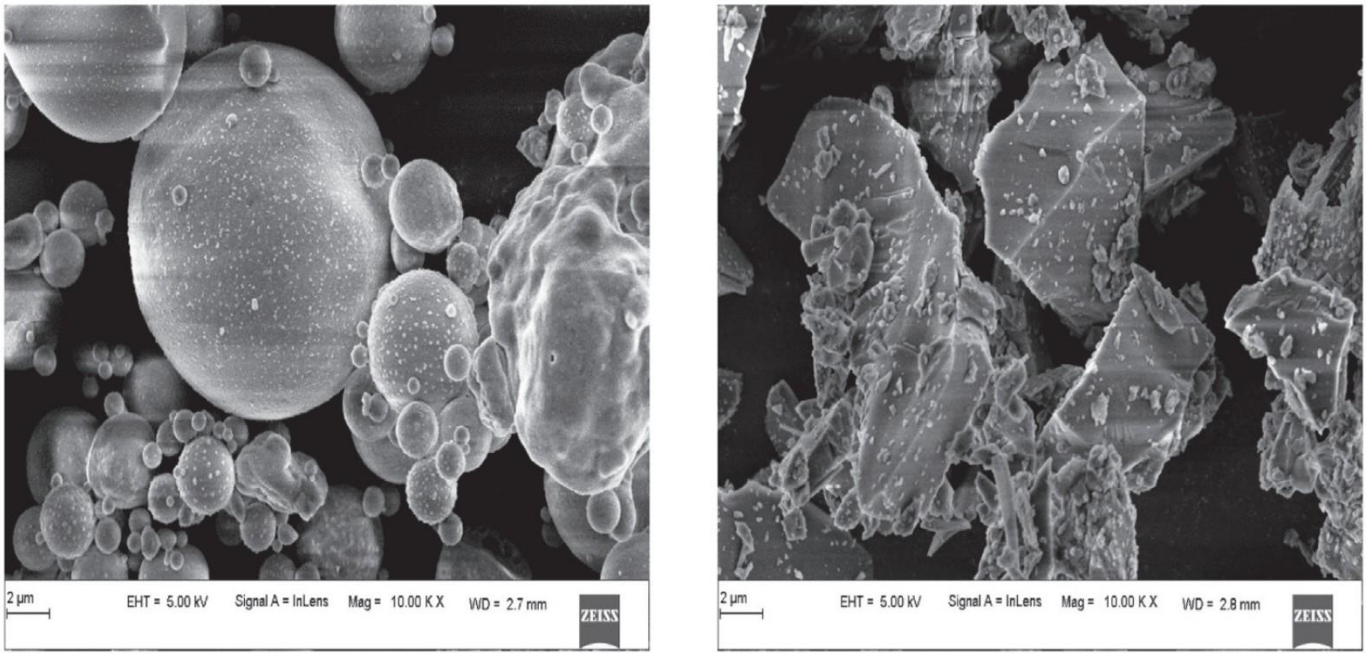

(a) (b)

Figure 1 Analysis of SEM (a) FA (b) GGBFS

In the preparation of geopolymer mortar, naturally sourced river sand was employed as the fine aggregate. The precursor materials were analyzed for their microstructural characteristics through scanning electron microscopy (SEM) and X-ray diffraction (XRD). As observed in the SEM micrographs (Fig. 1), the fly ash (FA) particles primarily displayed a smooth and spherical surface texture, whereas the ground granulated blast furnace slag (GGBFS) particles exhibited irregular and angular geometries [21]. Correspondingly, the XRD analysis (Fig. 2) indicated that both FA and GGBFS possessed a blend of amorphous and crystalline phases, confirming the heterogeneous nature of the raw binders.

Table 3 Alkali activator composition for Mix design

Mix id	Binder		Fiber		Sand	Solution	
	FA	GGBFS	PP	Steel		Na_2SiO_3	NaOH
G000	328.80	142.91	–	–	1163.82	131.20	56.10
P075G	328.80	142.91	2.14	–	1163.82	131.20	56.10
P125G	328.80	142.91	4.57	–	1163.82	131.20	56.10
P175G	328.80	142.91	7.11	–	1163.82	131.20	56.10
P225G	328.80	142.91	9.45	–	1163.82	131.20	56.10
P275G	328.80	142.91	11.759	–	1163.82	131.20	56.10
S075G	328.80	142.91	–	2.14	1163.82	131.20	56.10
S125G	328.80	142.91	–	4.57	1163.82	131.20	56.10
S175G	328.80	142.91	–	7.11	1163.82	131.20	56.10
S225G	328.80	142.91	–	9.45	1163.82	131.20	56.10
S275G	328.80	142.91	–	11.759	1163.82	131.20	56.10

(a) (b)

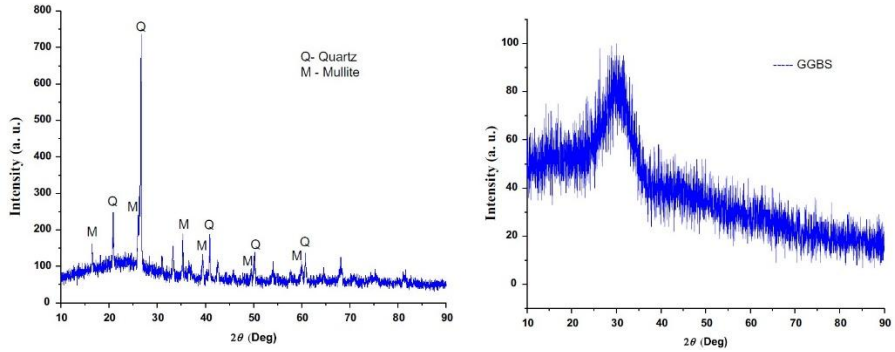

Figure 2 XRD Raw binders pattern used for experiments (a) FA (b) GGBS

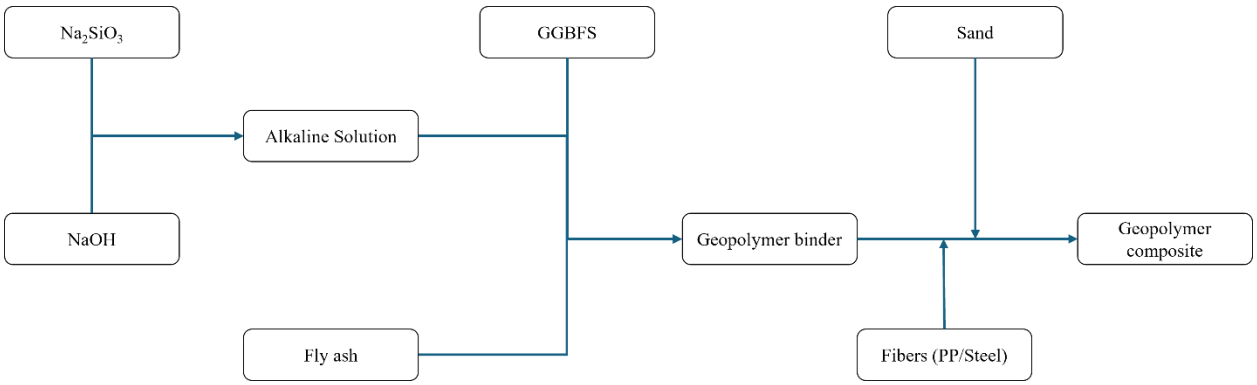

Figure 3 Mixing Procedure for the formation of alkali activator composite [22]

3. Mix Proportion

The alkali activator composite mixtures were designed following the mix proportioning guidelines reported in previous studies [23]. The detailed composition of materials used for producing the fiber-reinforced alkali activator mortars is presented in Table 3. The overall mixing sequence adopted for the preparation of the fiber-reinforced alkali activator mortar is illustrated in Figure 3.

PP and SF were incorporated individually into the alkali activator matrix at five different volume fractions: 0.75%, 1.0%, 1.75%, 2.0%, and 2.5%. Mix identifications were denoted as PP for polypropylene fiber–reinforced specimens and ST for SF–reinforced specimens. The selected dosage range was determined based on recommendations from earlier literature [30, 38, 39], allowing for a direct comparison of the mechanical performance between the two fiber types at equivalent inclusion levels.

4. Different Criteria for Casting, Curing, Testing

The influence of fiber inclusion on the flow characteristics of geopolymer composites was examined using the flow table method in accordance with ASTM C1437-20 [24]. Freshly prepared geopolymer mortar was poured into a truncated conical mold having dimensions of 70 mm (top diameter), 100 mm (bottom diameter), and 50 mm (height). After carefully lifting the mold, the spread diameter of the mixture was recorded, and the flow percentage was determined using Equation (1)

To evaluate the CS, cube specimens measuring 50 × 50 × 50 mm were cast following ASTM C109/C109M-20b [25]. The splitting tensile strength was measured on cylindrical samples (50 mm diameter × 100 mm height) as per ASTM C1006/C1006M-20. Similarly, flexural strength was assessed on prismatic beams (40 × 40 × 160 mm) under third-point loading conditions, in line with ASTM C293/C293M–16 [26].

The flexural toughness of fiber-reinforced geopolymer mortars was calculated from the area under the load–deflection curve obtained during the flexural test. The procedure was performed following ASTM C1018-97 [27], The corresponding toughness index was computed using Equation (2), where the displacement at the first visible crack was recorded. All mechanical tests were carried out after 28 days of ambient curing, and the average of three specimens was reported for each mixture.

For all mixes, PP and SF were incorporated separately in volume fractions of 0.75%, 1.0%, 1.75%, 2.0%, and 2.5%, relative to the total binder content. The fresh geopolymer mixes were cast into appropriate molds and compacted to remove air voids. After 24 hours, the specimens were demolded and cured under ambient laboratory conditions, maintaining a temperature between 24–35 °C and a relative humidity of about 67%, until testing.

The bulk density of the geopolymer composites was measured after 28 days of curing, following ASTM C20-00 (2015) [28]. The specimens were weighed in saturated, suspended, and oven-dried states. For saturation, the samples were immersed in demineralized water, boiled for 2 hours, and subsequently placed under vacuum for 24 hours. The dry mass was recorded after oven drying at 92 °C for 24 hours, and Equation (3) was used to determine the relative density.

Mechanical properties—namely compressive, splitting tensile, and flexural strengths—were measured at both 7 and 28 days to evaluate the development of strength with curing age. Furthermore, the static modulus of elasticity in compression was determined on 50 × 100 mm cylindrical specimens after 28 days of ambient curing, using a universal testing machine in accordance with ASTM C469M–14 [29].

Post-compression testing, the fractured samples were collected for microstructural characterization through scanning electron microscopy (SEM), X-ray diffraction (XRD), and energy-dispersive X-ray spectroscopy (EDS). These analyses were conducted to examine the morphology, phase composition, and fiber–matrix interfacial behavior of the geopolymer composites.

$$R = \frac{T - T_O}{T_O} * 100 \quad (1)$$

Where, R=flow variation in percentage (%)

T = the mean base diameter of the binder specimen after testing

T_o = initial base diameter prior to testing

$$a = \frac{E_b}{\delta_{tb}} X \frac{H}{b * h^2} \quad (2)$$

Where, Eb = flexural toughness measured at a deflection corresponding to 1/1501/1501/150 of the specimen span

δ_{tb} = deflection value at that same 1/1501/1501/150 span ratio,

are the specimen's length, width, and height (in mm)

$$T_O = 1 - \frac{T_t - T_b}{T_t} * 100 \quad (3)$$

Where, T_b = bulk density of the composite.
T_t = theoretical density, calculated from constituent properties= $T_g \times F_g + T_f \times T_f$
T_g = 28th day density of alkali activator
F_g = volumetric proportion (%) of the alkali activator
T_f = Specific gravity of fiber
T_f = corresponding fiber dosage expressed in volume percentage

5. Results and Discussion

5.1. Bulk density

Figures 4 and 5 illustrate the variation in bulk density of FA–GGBFS-based geopolymer composites incorporating different fiber contents after 28 days of ambient curing. As observed in Figure 5, an increase in polypropylene (PP) fiber dosage results in a progressive reduction in bulk density. This trend can be attributed to the lower specific gravity of PP fibers relative to the geopolymer binder. In contrast, the inclusion of steel fibers leads to a gradual increase in bulk density, which is consistent with their higher specific gravity compared to the surrounding matrix.
However, as the dosage of both PP and SF increased, a slight reduction in relative density was observed, as presented in Figure 5. This decrease was primarily associated with incomplete compaction at higher fiber contents, where fiber agglomeration and reduced flowability introduced microvoids within the matrix. The reduction effect was more pronounced in mixtures containing PP fibers beyond 2% volume fraction, suggesting that excessive PP fiber addition impairs matrix densification more severely than SF.

5.2. Compressive Strength

Figure 6 presents the compressive strength (CS) development of polypropylene (PP) and steel fiber (SF)-reinforced alkali-activated composites after 7 and 28 days of ambient curing. The incorporation of PP fibers resulted in a slight decline in compressive strength compared to the control specimen, while the mixes containing steel fibers showed a consistent enhancement in strength at both curing ages. Among all the formulations, the S225G.5 mixture exhibited the maximum compressive strength, reaching 61.75 MPa after 28 days of curing.

In general, steel fiber-reinforced alkali activator composites demonstrated superior compressive performance compared with PP fiber-based counterparts. Some PP fiber mixtures showed slightly improved strength at lower dosages (up to 2%), but further increases in fiber content resulted in a decline in CS. This reduction was attributed to difficulties in mixing, compaction, and vibration during specimen preparation, which likely introduced voids and reduced the fiber–matrix bond strength. The decrease in density with increasing PP fiber dosage also contributed to this reduction in CS. At higher PP fiber contents, deadhesion fibers and the alkali activator paste became more prevalent, further weakening the structural integrity of the matrix.
In contrast, the inclusion of SF up to a 2.5% volume fraction consistently improved CS. The boostd performance of steel fiber-reinforced specimens can be ascribed to the stronger interfacial bond between the fibers and the alkali activator binder, which provides greater resistance to crack propagation and internal spalling under load.
The strength improvement ratio (IR) values summarized in Table 4 further substantiate these findings. All PP fiber mixes exhibited negative IR values at 28 days, indicating a reduction in CS relative to the control mix. Specifically, mixes P075G, P125G, P125G.5, P225G, and P225G.5 recorded IR values of −8.64%, −6.45%, −3.74%, −0.26%, and −9.89%, respectively. Conversely, steel fiber-reinforced alkali activator mortars exhibited positive IR values, with S075G, S125G, S125G.5, S225G, and S225G.5 showing improvements of 1.66%, 4.00%, 6.26%, 9.83%, and 13.26%, respectively. These results confirm that steel fiber inclusion boosts CS, while PP fibers primarily contribute to toughness and post-cracking behavior rather than strength development.

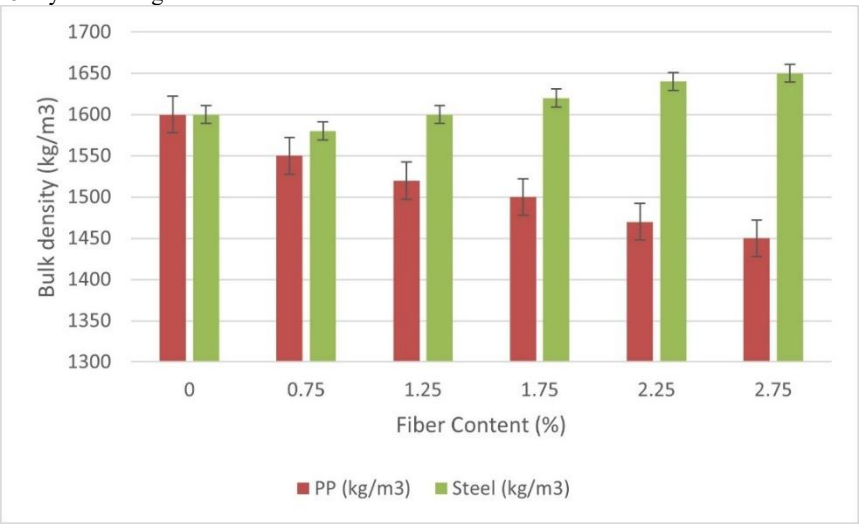

Figure 4 Variance in bulk density in alkali activator sample using fiber

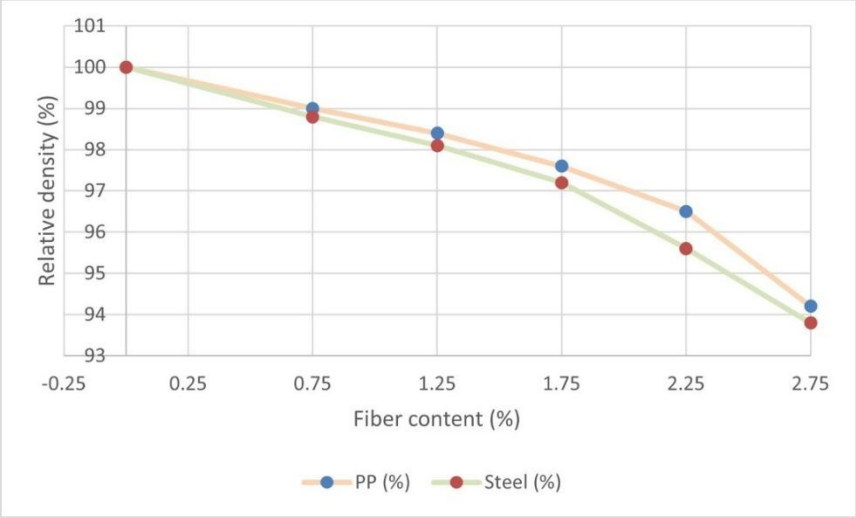

Figure 5 Variance in relative density of alkali activator sample using fiber

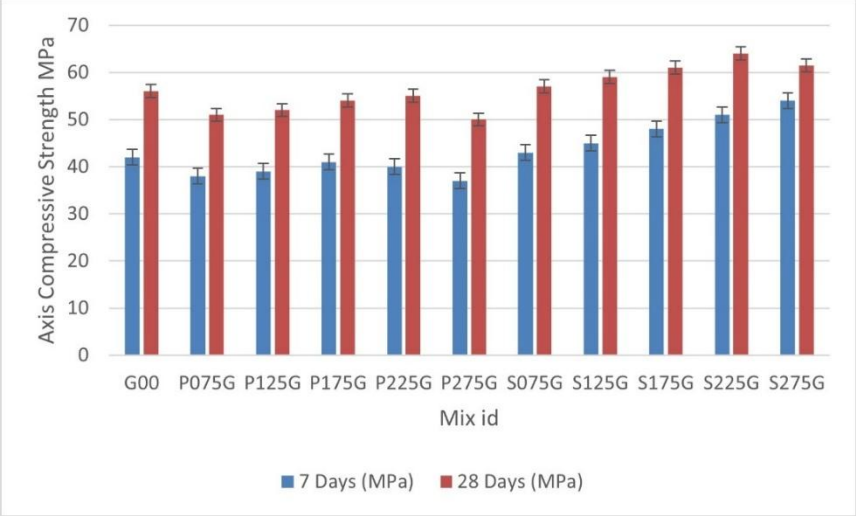

Figure 6 CS of alkali activator composites using fiber

Table 4 Strength improvement ratio of alkali activator samples

Mix	CS		Splitting Tensile Strength		Flexural Strength	
	Strength MPa	Improved Ratio %	Strength MPa	Improved Ratio %	Strength MPa	Improved Ratio %
G000	52.2	-	4.51	-	8.74	-
P075G	44.21	-9.24	4.6	2.22	8.11	2.25
P125G	55.5	-7.15	4.72	5.55	7.89	6.69
P175G	56.8	-5.34	5.33	20.49	7.27	11.84
P225G	58.66	-0.756	6.12	16.35	8.16	29.16
P275G	49.43	-8.19	3.78	-4.19	6.62	-3.87
S075G	51.75	2.26	4.88	7.63	6.18	2.19
S125G	53.17	6	5.54	18.73	7.10	15
S175G	54.3	8.86	6.14	35.52	8.83	25.03
S225G	54.5	10.23	6.44	38.24	11.11	31.9
S275G	64.1	11.16	7.21	44.1	13.59	51.19

5.3. Splitting Tensile Strength

The splitting tensile strength characteristics of alkali-activated fiber composites, tested after 7 and 28 days of ambient curing, are shown in Figure 8. During testing, the control specimens without fiber reinforcement fractured abruptly at the ultimate load, producing a distinct cracking sound—typical of brittle failure. In contrast, the mixes containing either polypropylene (PP) or steel fibers displayed a gradual mode of failure, where fine surface cracks widened progressively until final rupture. Among the two fiber types, steel-reinforced composites exhibited less surface spalling than those with PP fibers, which can be attributed to the higher tensile strength and aspect ratio of steel fibers.

Introducing fibers clearly influenced the tensile response of the geopolymer composites. The inclusion of PP and steel fibers enhanced the splitting tensile strength by roughly 1.75–52 % in comparison with the control mortar. This improvement arises from the fibers' ability to restrain crack growth and transfer stress across developing cracks, allowing the matrix to sustain greater strain before failure and thereby reducing brittleness. Between the two reinforcements, the steel fibers consistently produced higher tensile capacity and greater resistance after cracking than the PP fibers.

As presented in Figure 8, the S225G.5 mixture—containing 2.25 % steel fiber—reached the maximum tensile strength of 8.52 MPa, whereas the P225G.5 mixture recorded the lowest value of 5.48 MPa at the same fiber fraction. This difference reflects the superior bond strength and stress-transfer efficiency of steel fibers relative to polypropylene.

The 28-day improvement ratios (IR) derived from experimental results are summarized in Table 4. All PP fiber composites exhibited comparatively small IR values, confirming only moderate strength improvement when compared with steel-reinforced counterparts. The IR values for P075G, P125G, P125G.5, P225G, and P225G.5 were 1.42 %, 3.74 %, 14.59 %, 28.65 %, and −2.49 %, respectively. The P225G mix achieved the highest increase among PP series, while further addition of PP fibers to 2.5 % caused a decline in strength, likely due to poor dispersion and void formation within the matrix.

Conversely, the geopolymer mortars reinforced with steel fibers showed a steady rise in strength with fiber addition, producing positive IR values at all levels—4.98 %, 18.33 %, 25.62 %, 34.34 %, and 51.60 % for S075G, S125G, S125G.5, S225G, and S225G.5, respectively. The S225G.5 mix again exhibited the highest improvement, confirming that a greater steel fiber content significantly enhances tensile strength and crack-bridging capability.

A clear influence of curing duration was also observed. Specimens tested at 28 days displayed notably higher tensile strength than those tested at 7 days, with an increase ranging between 40% and 65%. This progressive gain is attributed to the continued geopolymerization reaction, which results in a denser microstructure and improved fiber–matrix bonding. The same pattern of strength development was consistently reflected in the compressive and flexural strength results as well.

5.4. Flexural Strength

The flexural behavior of the fiber-reinforced alkali-activated composites was evaluated after 7 and 28 days of ambient curing. As illustrated in the results, incorporating both polypropylene (PP) and steel fibers noticeably enhanced the bending performance of the alkali-activated mortars compared with the plain mix. The presence of fibers increased the initial crack load and allowed the prisms to sustain greater stress before failure, demonstrating improved load-bearing capacity and post-crack resistance.

For the PP fiber-reinforced specimens, the maximum flexural strength—9.73 MPa—was recorded at a 2.35% fiber volume fraction after 28 days of curing. Beyond this limit, particularly at 2.25%, a slight decrease in flexural strength was observed. This reduction can be linked to difficulties during mixing and compaction at higher fiber contents, which may have led to the development of internal voids and weaker fiber–matrix adhesion. Additionally, the decrease in composite density at elevated PP fiber dosages further contributed to the decline in flexural strength. In contrast, the steel fiber-reinforced specimens exhibited a clear upward trend in flexural strength with increasing fiber dosage. The highest flexural strength, 12.15 MPa, was obtained for the S225G.5 mix after 28 days, whereas the corresponding 7-day strength was 8.95 MPa. These findings confirm the superior reinforcing effect of SF in improving flexural behavior, primarily due to their higher modulus of elasticity and better mechanical interlock with the alkali activator matrix.

Overall, while both fiber types improved the ductility and flexural response of the alkali activator composites, SF proved more effective in enhancing post-crack load resistance and energy absorption. The results clearly demonstrate that optimizing fiber volume fraction is essential to achieving balanced workability and mechanical performance in FA–GGBFS-based alkali activator mortars.

5.5. Flexural Toughness

The flexural toughness factor and mid-span deflection results of the fiber-reinforced alkali activator composites are summarized in Table 5. Incorporating fibers into the alkali activator matrix significantly boostd flexural performance compared to the unreinforced (control) mix, with steel fiber-reinforced specimens showing particularly pronounced improvements.

For polypropylene (PP) fiber-reinforced composites, the central deflection values increased by 30%, 50%, 133.33%, 176.67%, and 3.33% for the mixes P075G, P125G, P125G.5, P225G, and P225G.5, respectively, relative to the control sample. Although all PP fiber mixes displayed higher deflection capacities than the plain alkali activator, the most notable boostment occurred at 2.35%fiber content, beyond which a marginal decline was observed.

In contrast, steel fiber-reinforced alkali activator composites exhibited a more substantial increase in deflection and flexural toughness. The center deflection improved by 50%, 143.33%, 226.67%, 286.67%, and 360% for S075G, S125G, S125G.5, S225G, and S225G.5, respectively. This clearly indicates that SF provided more efficient crack-bridging and energy absorption mechanisms than PP fibers, contributing to a higher overall toughness.

As illustrated in Figure 7, both PP and SF improved the flexural toughness factor compared to the control mix [30]. The measured toughness factors for PP fiber-reinforced alkali activator composites were 0.95, 1.24, 1.63, 1.97, and 1.80 N/mm² for P075G, P125G, P125G.5, P225G, and P225G.5, respectively. Corresponding values for steel fiber-reinforced mixes were 1.05, 1.40, 1.86, 2.17, and 2.95 N/mm² for S075G, S125G, S125G.5, S225G, and S225G.5, confirming the superior reinforcement effect of SF.

Table 5 further demonstrates that the inclusion of SF markedly increased the flexural toughness percentage. The mix containing 2.25% SF (S225G.5) achieved the highest boostment, recording a 273.42% increase relative to the control mix. Conversely, the lowest toughness was observed for the P075G mix, primarily due to the limited fiber content, which provided insufficient crack-bridging action.

Overall, a positive correlation between fiber volume fraction and flexural toughness was observed for both fiber types. Nevertheless,

in PP fiber-reinforced composites, an excessive fiber dosage beyond 2% led to a minor decline in flexural performance, likely due to fiber agglomeration and reduced workability. Specifically, the toughness improvements for P225G and P225G.5 mixes were 149.37% and 127.85%, respectively, indicating that 2.35%PP fiber content is near the optimum level for achieving boostd flexural behavior in FA–GGBFS-based alkali activator composites.

Table 5 Deflection and flexural toughness of alkali activator samples using fiber

Mix id	Ultimate strength (MPa)	Deflection at centre (mm)	Flexural toughness factor (N/ mm^2)	Increase in deflection (%)	Increase in flexural toughness (%)
G000	8.8	0.4	0.89	–	–
P075G	8.95	0.49	0.75	31	21.15
P125G	9.13	0.755	1.44	51	55.16
P175G	9.55	0.67	1.753	132.01	103.53
P225G	8.63	0.73	1.87	175.57	144.27
P275G	7.69	0.41	1.9	4.13	123.45
S075G	7.63	0.755	1.1	51	37.61
S125G	9.37	0.83	1.75	141.13	78.12
S175G	10.15	0.78	1.96	227.77	133.14
S225G	11.88	1.66	2.57	289.67	177.58
S275G	13.25	1.78	2.99	364	272.62

Table 6 Predicted compressive elastic modulus values

Mix id	CS (MPa)	Mean Density of GPC Kg/m^3	Compressive elastic modulus (GPa)			
			ACI 318-14	AS 3600, 2009	Bellum et al.,[22]	This paper
G000	53.3	2168	31.986	30.189	27.762	26.662
P075G	48.61	2115	29.459	28.320	31.658	32.758
P125G	51.8	2074	28.948	27.693	32.116	33.216
P175G	53.4	2037	28.617	27.204	33.868	34.968
P225G	59.16	2006	28.432	26.849	34.723	35.623
P275G	47.93	1958	26.060	25.124	32.478	33.578
S075G	58.2	2152	31.893	30.003	29.589	30.689
S125G	59.47	2128	31.720	29.705	32.796	33.896
S175G	56.7	2095	31.321	29.207	33.924	34.824
S225G	58.64	2051	30.845	28.577	34.782	35.882
S275G	66.5	2007	30.320	27.924	35.843	36.943

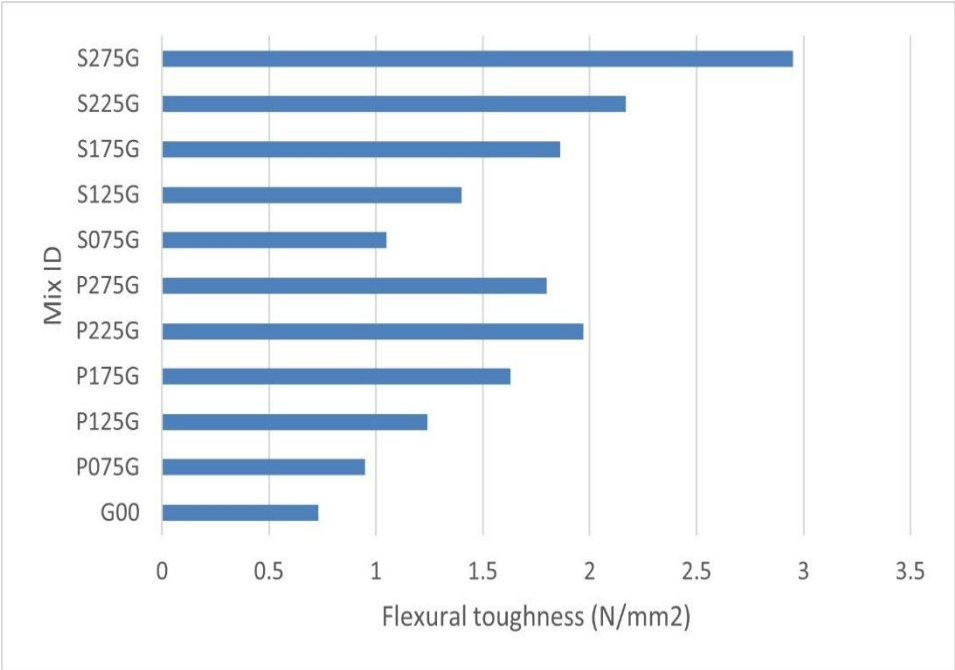

Figure 7 Flexural toughness of alkali activator samples

5.6. Elastic modulus

Table 6 summarizes the compressive elastic modulus values obtained for polypropylene (PP) and steel fiber (SF)-reinforced alkali-activated composites. A clear trend of increasing stiffness with rising fiber dosage was observed for both fiber types. After 28 days of ambient curing, the elastic modulus values for the PP series—G000, P075G, P125G, P125G.5, P225G, and P225G.5—were recorded as 26.662, 32.758, 33.216, 34.968, 35.823, and 33.578 GPa, respectively. Similarly, the steel fiber-reinforced mixes—S075G, S125G, S125G.5, S225G, and S225G.5—achieved modulus values of 30.689, 33.896, 34.824, 35.882, and 36.943 GPa, respectively.

The addition of fibers considerably enhanced the stiffness characteristics of the composites when compared with the unreinforced control mix. This improvement is primarily associated with the improved load transfer mechanism and the enhanced fiber–matrix interfacial bond, both of which help constrain the deformation of the composite under compressive loading. Within the PP fiber group, the highest elastic modulus (34.723 GPa) was attained at a 2% fiber volume fraction. A marginal reduction beyond this level was noted, likely due to fiber clustering and the formation of localized voids within the matrix. In contrast, the steel fiber-reinforced specimens displayed a steady and continuous rise in elastic modulus with increasing fiber dosage, reaching a maximum of 35.843 GPa at 2.5% fiber content. This consistent enhancement highlights the superior reinforcing capacity of steel fibers, which promote better stress redistribution and greater resistance to microcrack initiation under compression.

The compressive elastic modulus of the fiber-reinforced composites was also estimated theoretically using Equation (4), which relates the modulus to the corresponding compressive strength (CS) values. A comparison between the calculated and experimental results is depicted in Figure 8, representing the proposed predictive model for estimating the elastic modulus (in GPa) after 28 days of ambient curing. The predicted data closely matched the experimental observations, as shown in Table 6, with the regression coefficient (R^2) approaching unity. This strong correlation confirms the validity and reliability of the developed empirical model for forecasting the elastic behavior of fiber-reinforced alkali-activated composites.

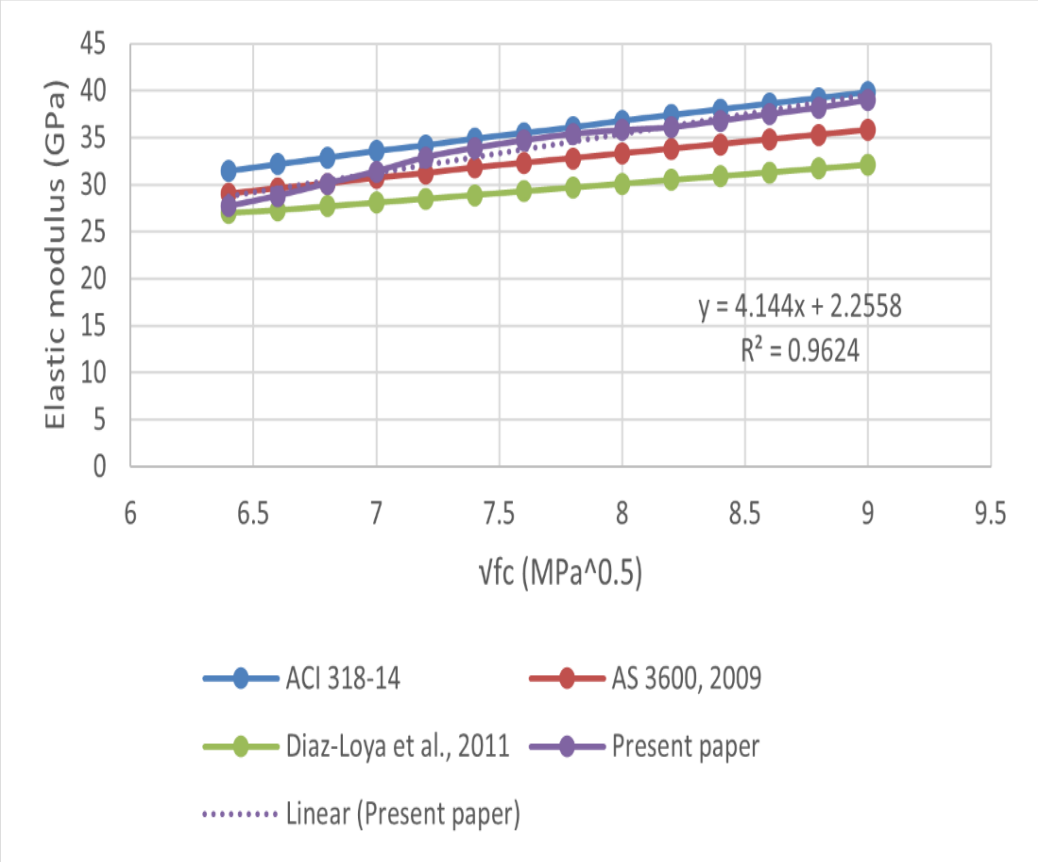

Figure 8 Equation for Elastic Modulus

The proposed equation can be expressed as:

$$E_c = 0.000040 * \rho^{1.75}\sqrt{f_c} \quad (4)$$

Where, E_c is the compressive elastic modulus (GPa),
ρ is the bulk density (kg/m³), and
f_c is the CS (MPa)

Among all tested mixtures, the alkali activator composite containing 2.75% SF exhibited the highest compressive elastic modulus, confirming the beneficial influence of steel fiber addition on stiffness boostment. The FA–GGBFS-based matrix reinforced with SF demonstrated improved load transfer efficiency and reduced microcrack propagation, resulting in a higher elastic modulus compared with both the control and PP fiber-reinforced samples.

6. Conclusion

This study examined the mechanical and microstructural performance of FA–GGBFS-based alkali activator composites reinforced with PP and SF. The mechanical properties, including compressive, splitting tensile, and flexural strengths, were assessd along with microstructural features such as fiber–matrix bonding and debonding. The principal findings are summarized below:

- Adding fibers made the alkali activator mixes harder to work with. The flowability dropped by about 64.1% for PP fibers and 67.5% for SF compared to the control mix. When fiber content increased to 2.75% by volume, the bulk density went down by 7.35% in PP fiber composites, but it went up by 5.37% in steel fiber mixes compared to the control specimen.
- Adding fibers greatly improved the bending strength of alkali activator composites. After 28 days, the PP and steel fiber-reinforced samples showed strength increases of 28.18% and 52.12%, respectively, compared to the mix without fibers. Similarly, adding SF improved CS by 18.16% after 28 days.
- Fiber addition also boosted the bending toughness of alkali activator composites. The PP fiber-reinforced sample with 2% volume showed a 152.27% improvement, while the steel fiber-reinforced sample with 2.75% volume showed a 278.18% increase compared to the control mix. These results show that fiber reinforcement is effective in improving energy absorption and flexibility after cracking.

Overall, the incorporation of steel and PP fibers markedly boostd the mechanical performance and toughness of FA–GGBFS-based alkali activator composites. SF were found to be more effective than PP fibers in improving strength, stiffness, and crack resistance, making them suitable for structural applications requiring improved ductility and durability.

7. References

[1] GCCA-2025, "Cement Industry Net Zero Progress Report 2024/2025," Action & Progress, UN, 2025.

[2] R. M. Andrew, "Global CO2 emissions from cement production," Earth System Science Data, vol. 10(1), pp. 195-217, 2018.

[3] F. Althoey, W. S. Ansari and M. &. D. A. F. Sufian, "Advancements in low-carbon concrete as a construction material for the sustainable built environment.," Developments in the built environment, vol. 16, p. 100284, 2023.

[4] A. H. Ismail, A. Kusbiantoro, Y. Tajunnisa and J. J. &. L. I. Ekaputri, "A review of aluminosilicate sources from inorganic waste for geopolymer production: Sustainable approach for hydrocarbon waste disposal.," Cleaner Materials, vol. 13, p. 100259., 2024.

[5] &. A. M. Adnan, "Geopolymer concrete as a sustainable alternative to OPC.," Journal of Umm Al-Qura University for Engineering and Architecture, pp. 1-23, 2025.

[6] N. Shehata, O. A. Mohamed, E. T. Sayed and M. A. &. O. A. G. Abdelkareem, "Geopolymer concrete as green building materials: Recent applications, sustainable development and circular economy potentials.," Science of the Total Environment, vol. 836, p. 155577, 2022.

[7] S. Ruan, R. Gao, W. Tu and D. &. Z. M. Yan, "Alkali-activated materials with organics: A critical review.," Composites Part B: Engineering, vol. 284, p. 111712, 2024.

[8] A. E. &. S. A. P. Alexander, "Studies on the microstructure and durability characteristics of ambient cured FA-GGBS based geopolymer mortar.," Construction and Building Materials, vol. 347, p. 128538, 2022.

[9] A. K. F. Gaddafi, "Impact of ground granular blast slag proportioning in fly ash geopolymer mortars with eco-processed pozzolana and palm oil clinker sand.," Discover Materials, vol. 5(1), p. 57, 2025.

[10] A. K. HM and M. S. Shoba, "Durability and microstructure of fiber-reinforced geopolymer concrete with FA and GGBS.," Structures , vol. 71, p. 108096, 2025.

[11] N. Ganesan, R. Abraham and S. D. Raj, "Durability characteristics of steel fibre reinforced geopolymer concrete," Construction and Building Materials,, vol. 93, pp. 471-476., 2015.

[12] S. Bernal, R. De Gutierrez, S. Delvasto and E. Rodriguez, "Performance of an alkali-activated slag concrete reinforced with steel fibers," Construction and building Materials, vol. 24(2), pp. 208-214, 2010.

[13] A. Islam, U. J. Alengaram, M. Z. Jumaat, N. B. Ghazali, S. Yusoff and I. I. Bashar, "Influence of steel fibers on the mechanical properties and impact resistance of lightweight geopolymer concrete.," Construction and Building Materials, vol. 152, pp. 964-977, 2017.

[14] A. Bhutta, P. H. Borges, C. Zanotti, M. Farooq and N. Banthia, "Flexural behavior of geopolymer composites reinforced with steel and polypropylene macro fibers.," Cement and Concrete Composites, vol. 80, pp. 31-40, 2017.

[15] F. Xu, X. Deng, C. Peng, J. Zhu and J. Chen, "Mix design and flexural toughness of PVA fiber reinforced fly ash-geopolymer composites.," Construction and Building Materials, vol. 150, pp. 179-189, 2017.

[16] F. Xu, X. Deng, C. Peng, J. Zhu and J. Chen, "Mix design and flexural toughness of PVA fiber reinforced fly ash-geopolymer composites.," Construction and Building Materials, vol. 150, pp. 179-189, 2017.

[17] K. Kishore and R. Tomar, "Understanding the role of interfacial transition zone in cement paste and concrete.," Materials Today: Proceedings, vol. 80, pp. 877-881, 2023.

[18] E. K. Fayed, A. M. El-Khayatt, F. I. El-Hosiny, M. Ghareb, W. M. Abd El-Gawad, A. Sabik and H. A. Abdel-Gawwad, "Alkali-activated concrete waste powder-based coating: Preparation, performance, and electrochemical resistance.," Developments in the Built Environment, p. 100714, 2025.

[19] A. C618, "Standard Specification for Coal Fly Ash and Raw or Calcined Natural Pozzolan for Use in Concrete," ASTM, 2019.

[20] A. C989/C989M, "Standard Specification for Slag Cement for Use in Concrete and Mortars," ASTM, 2017.

[21] F. Chen, J. Zhao, B. Zhang, Y. Feng, C. Chen, Z. Lu and J. Xie, "Physical, mechanical and microstructural properties of ultra-lightweight high-strength geopolymeric composites.,"

ase Studies in Construction Materials, vol. 19, p. 02446, 2023.

[22] R. R. Bellum, "Influence of steel and PP fibers on mechanical and microstructural properties of fly ash-GGBFS based geopolymer composites.," Ceramics International, vol. 48(5), pp. 6808-6818, 2022.

[23] D. N. S. P. J. L. &. S. M. Bondar, "Efficient mix design of alkali activated slag concretes based on packing fraction of ingredients and paste thickness.," Journal of cleaner production, vol. 218, pp. 438-449, 2019.

[24] A. C1437, "Standard Test Method for Flow of Hydraulic Cement Mortar," ASTM, 2020.

[25] A. C109/C109M, "Standard Test Method for Compressive Strength of Hydraulic Cement Mortars (Using 2-in. or [50 mm] Cube Specimens)," ASTM, 2020.

[26] A. C293/C293M, "Standard Test Method for Flexural Strength of Concrete (Using Simple Beam With Center-Point Loading) (Withdrawn 2025)," ASTM, 2016.

[27] A. C1018, "Standard Test Method for Flexural Toughness and First-Crack Strength of Fiber-Reinforced Concrete (Using Beam With Third-Point Loading) (Withdrawn 2006)," ASTM, 1997.

[28] A. C20-00, "Standard Test Methods for Apparent Porosity, Water Absorption, Apparent Specific Gravity, and Bulk Density of Burned Refractory Brick and Shapes by Boiling Water," ASTM, 2022.

[29] A. C469/C469M, "Standard Test Method for Static Modulus of Elasticity and Poisson's Ratio of Concrete in Compression," ASTM, 2014.